Baiu Rainband Termination in Atmospheric and Coupled Atmosphere–Ocean Models

AKIRA KUWANO-YOSHIDA AND BUNMEI TAGUCHI

Earth Simulator Center, Japan Agency for Marine-Earth Science and Technology, Yokohama, Kanagawa, Japan

SHANG-PING XIE

International Pacific Research Center, and the Department of Meteorology, University of Hawai'i at Mānoa, Honolulu, Hawaii, and Scripps Institution of Oceanography, University of California, San Diego, La Jolla, California

(Manuscript received 15 April 2013, in final form 3 August 2013)

ABSTRACT

The baiu rainband is a summer rainband stretching from eastern China through Japan toward the northwestern Pacific. The climatological termination of the baiu rainband is investigated using the Japanese 25-yr Reanalysis (JRA-25), a stand-alone atmospheric general circulation model (GCM) forced with observed sea surface temperature (SST) and an atmosphere–ocean GCM (AOGCM). The baiu rainband over the North Pacific abruptly shifts northward and weakens substantially in early July in the atmospheric GCM (AGCM), too early compared to observations (late July). The midtroposphere westerly jet and its thermal advection explain this meridional shift of the baiu rainband, but the ocean surface evaporation modulates the precipitation intensity. In AGCM, deep convection in the subtropical northwestern Pacific sets in prematurely, displacing the westerly jet northward over the cold ocean surface earlier than in observations. The suppressed surface evaporation over the cold ocean suppresses precipitation even though the midtropospheric warm advection and vertically integrated moisture convergence are similar to those before the westerly jet's northward shift. As a result, the baiu rainband abruptly weakens after the northward shift in JRA-25 and AGCM. In AOGCM, cold SST biases in the subtropics inhibit deep convection, delaying the poleward excursion of the westerly jet. As a result, the upward motion induced by both the strong westerly jet and the rainband persist over the northwestern Pacific through summer in the AOGCM. The results indicate that the westerly jet and the ocean evaporation underneath are important for the baiu rainband, the latter suggesting an oceanic effect on this important phenomenon.

1. Introduction

The baiu is a quasi-stationary rainband over East Asia and the northwestern Pacific in early summer between June and July, often characterized as a subtropical front in moisture between the tropics and extratropics (Ninomiya 1984; Ninomiya and Akiyama 1992). The baiu rainband shows multiscale structures from meso- to synoptic scales (Ninomiya and Akiyama 1992). Because of the multiscale nature, the baiu rainband provides much needed rainfall to supply precious water to a broad region of East Asia, causing local disasters such as floods and mudslides by heavy rain.

Recently Sampe and Xie (2010) proposed a hypothesis linking the subtropical jet and baiu rainband. They suggest that horizontal warm advection by the subtropical jet induces upward motion in the midtroposphere using the thermodynamic energy equation. Specifically, the warm air mass over the Tibetan Plateau flows westward on the upper jet over East Asia, and the adiabatic ascent on isentropic surfaces triggers convection in the baiu rainband. Transient disturbances propagating from the Asian continent further aid convection along the jet. Latent heating within the baiu rainband modifies the upward motion strength. Kosaka et al. (2011) show that the hypothesis explains the interannual variability in the baiu rainband qualitatively.

Although much progress has been made in understanding the baiu rainband, several important questions remain. The seasonal termination of the baiu rainband is an unsolved issue. The baiu rainband gradually moves northward in mid-July and abruptly terminates around

Corresponding author address: Akira Kuwano-Yoshida, Earth Simulator Center, Japan Agency for Marine-Earth Science and Technology, 3173-25 Showa-machi, Kanazawa-ku, Yokohama, Kanagawa 236-0001, Japan.
E-mail: akiray@jamstec.go.jp

DOI: 10.1175/JCLI-D-13-00231.1

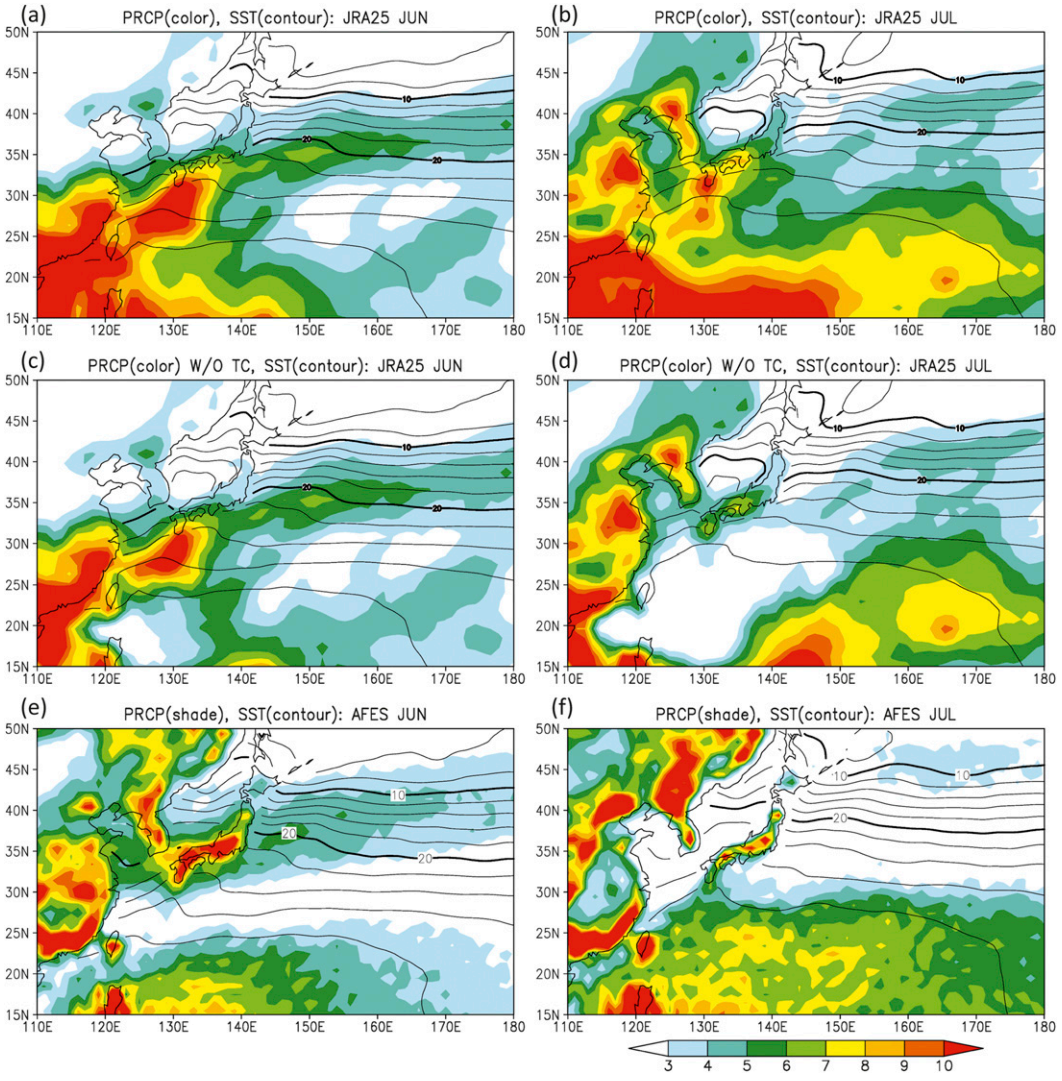

FIG. 1. Climatological precipitation (color, mm day^{-1}) and SST (contour interval is 2°C with 10° and 20°C contours thickened) in (left) June and (right) July: (a),(b) JRA-25, (c),(d) JRA-25 without precipitation associated with tropical cyclones, and (e),(f) AFES.

late July (Saito 1985; Sampe and Xie 2010). Saito (1985) suggested that weakening of the upper trough occurs at baiu termination over Japan. Ueda et al. (1995) and Ueda and Yasunari (1996) proposed that "the subtropical convection jump" causes a Rossby wave train and triggers the abrupt baiu termination. The subtropical convective jump is an abrupt northward shift of large-scale convective activity over the western Pacific around 20°N, 150°E in late July. In addition the shift is associated with tropical cyclone activity. The convective jump, however, does not appear clearly every year. Ueda and Yasunari (1996) reported that the typical convective jump rarely occurs in El Niño years. While Ueda et al. (2009) suggest that atmospheric moistening may cause the subtropical convection jump rather than local SST, the mechanism has not been fully understood.

Another question is the origin of pronounced rainfall in the baiu front. The moisture transport is considered important by the southwesterly flow on the western flank of the North Pacific subtropical high and the westerly flow from the Bay of Bengal (Akiyama 1973; Kodama 1992). Matsumoto et al. (1971) suggest that the moisture transport from the south makes a larger contribution to precipitation over the East China Sea than over the Japanese mainland. Since environment moisture influences the development of atmospheric disturbances in the baiu front (Tochimoto and Kawano 2012), it is important to clarify the relative roles of local moisture supply (e.g.,

evaporation) and large-scale environmental transport in supporting the baiu rainband. Recent high-resolution observations of precipitation, sea surface temperature (SST), and surface winds from satellites provide more detailed structure of the baiu rainband. Sasaki et al. (2012) report that strong surface evaporation and surface convergence associated with the local SST maximum along the Kuroshio strengthens baiu precipitation over the East China Sea.

Atmospheric general circulation models (AGCMs) and atmosphere–ocean GCMs (AOGCMs) have been used to simulate and predict the baiu rainband. Ninomiya et al. (2002) report features of ''baiu phase'' and ''non-baiu phase'' in an AGCM, suggesting that the upper jet, moisture flux, and synoptic disturbances are important to reproduce the baiu front, even if the continent–ocean thermal contrast is reasonably maintained in the model. Kawatani and Takahashi (2003) examine dependency on model resolution and cumulus parameterization of baiu reproducibility in an AGCM. They suggest the importance of the subtropical jet strength and an early termination of the baiu front in the AGCM, regardless of cumulus parameterizations. Ninomiya (2009) reports large diversity of baiu representation among current CGCMs in the World Climate Research Programme's Coupled Model Intercomparison Project phase 3 (CMIP3; Meehl et al. 2007). Although these studies note the importance of the subtropical jet for baiu rainband maintenance, they do not offer specific mechanisms for this relationship.

The present study investigates the seasonal evolution of the baiu rainband using a reanalysis and a pair of AGCM and AOGCM. Each model shows a distinct seasonal march of the baiu rainband from the other, providing a unique opportunity to understand the mechanism of the baiu rainband maintenance and termination. We show that in both reanalysis and models, the seasonal march mostly follows that of the zonal jet through the midtroposphere warm advection mechanism. The precipitation amount, however, corresponds less well with the warm advection forcing. The moisture budget analysis shows that local evaporation under and south of the baiu rainband is important for the precipitation amount. After the baiu termination, the northward shifted jet is located over the cold SST north of the Kuroshio–Oyashio Extension, and weak evaporation from the sea surface reduces the baiu rainfall amount even though the midtroposphere warm advection continues to force upward motion.

The rest of the paper is organized as follows: The description of the models and data are presented in section 2, followed by an overview of the baiu seasonal march in the AGCM and observations (section 3).

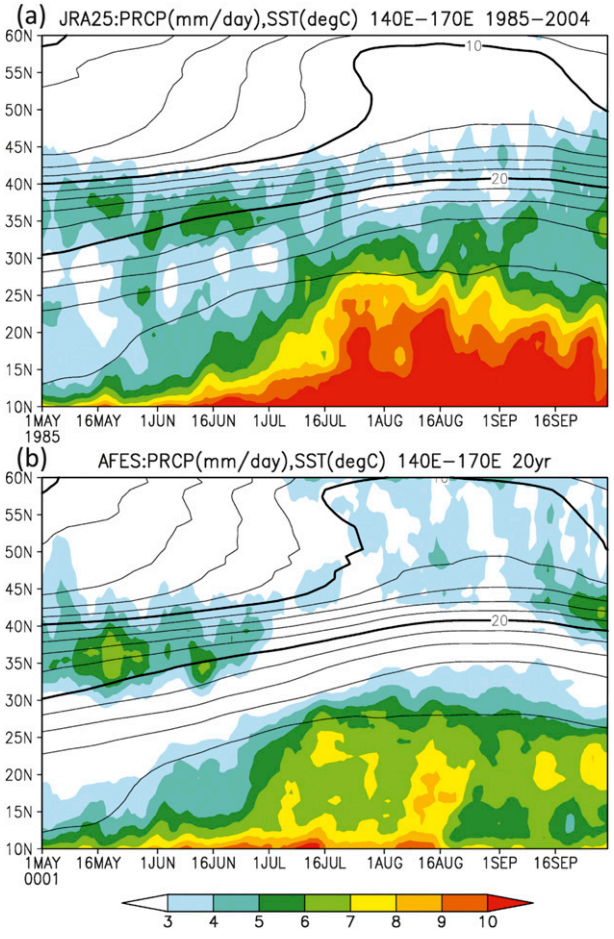

FIG. 2. Daily climatology of precipitation (color, mm day^{-1}) and SST (contour interval is 2°C with 10° and 20°C contours thickened) averaged between 140° and 170°E with 5-day running mean of (a) JRA-25 and (b) AFES from 1 May to 30 September.

Section 4 analyzes the baiu rainband termination, and section 5 presents the moisture budget analysis of the baiu rainband. Section 6 discusses the baiu rainband mechanisms in the AOGCM, and section 7 gives concluding remarks.

2. Data and methods

We use two models: the AGCM for the Earth Simulator (ES), version 3 (AFES; Ohfuchi et al. 2004, 2007; Enomoto et al. 2008; Kuwano-Yoshida et al. 2010a), and the coupled atmosphere–ocean GCM for the Earth Simulator (CFES; Komori et al. 2008; Taguchi et al. 2012), which consists of AFES and the Coupled Ocean–Sea Ice Model for the ES (OIFES; Komori et al. 2005). AFES is based on the Center for Climate System Research/National Institute for Environmental Studies (CCSR/NIES) AGCM, version 5.4.02 (Numaguti et al.

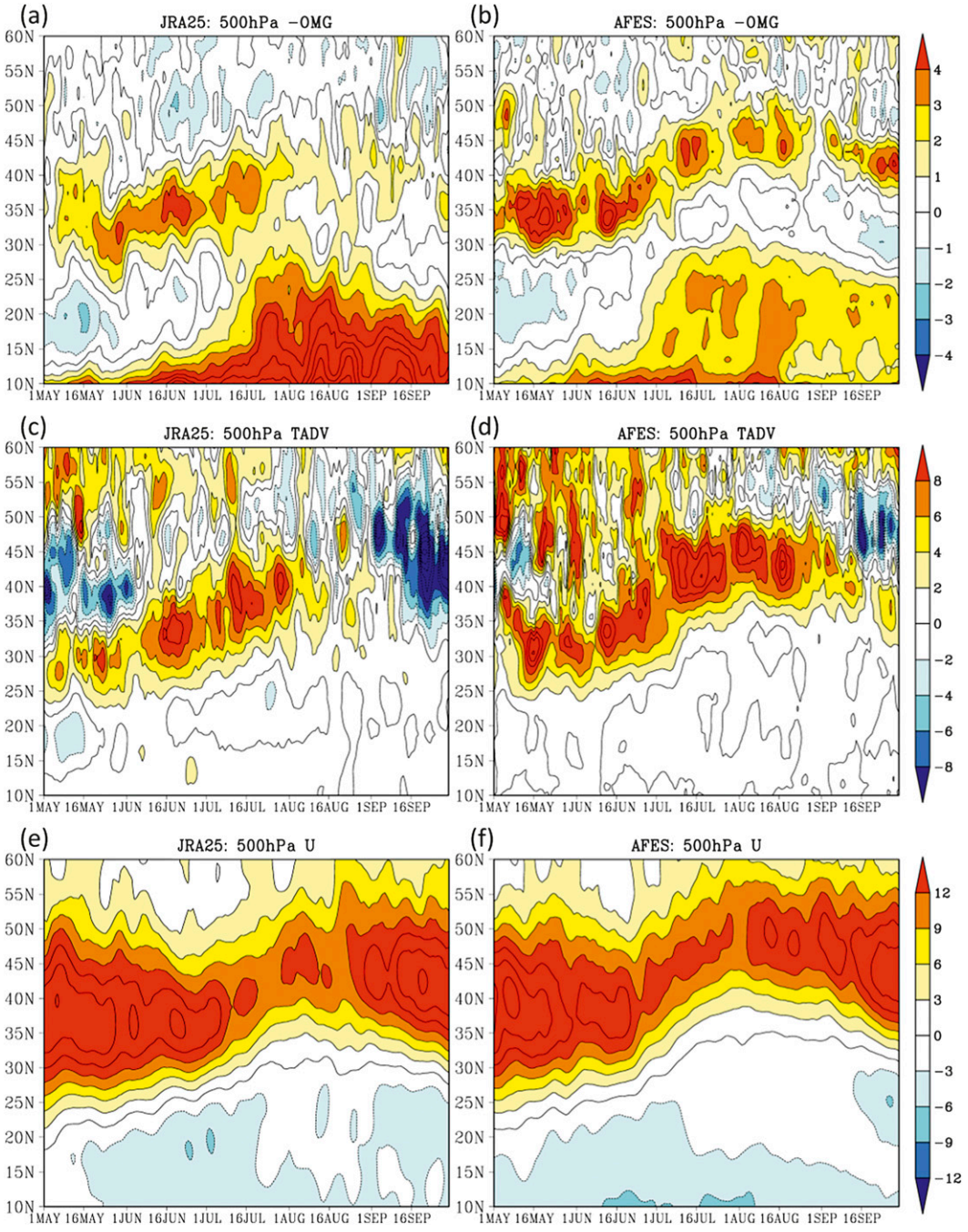

FIG. 3. As in Fig. 2, but for (a),(b) vertical pressure velocity with negative sign (10^{-2} Pa s^{-1}), (c),(d) horizontal temperature advection (10^{-6} K s^{-1}), and (e),(f) zonal wind (m s^{-1}) at 500 hPa for (left) JRA-25 and (right) AFES.

1997), while OIFES is based on the Modular Ocean Model, version 3 (MOM3; Pacanowski and Griffies 2000). Computational codes of AFES and OIFES have been substantially rewritten from their prototypes in order to attain their high computational efficiency on the particular architecture of ES and to implement improved parameterizations of physical processes. The models have medium horizontal resolution, T119 spectral truncation (equivalently 100-km grid intervals) with 48 levels for AFES, and 0.5° grid intervals with 54 vertical levels for OIFES (Taguchi et al. 2012). The initial conditions of the atmosphere and ocean are climatology at 0000 UTC 1 January from the 40-yr European Centre for Medium-Range Weather Forecasts (ECMWF) Re-Analysis

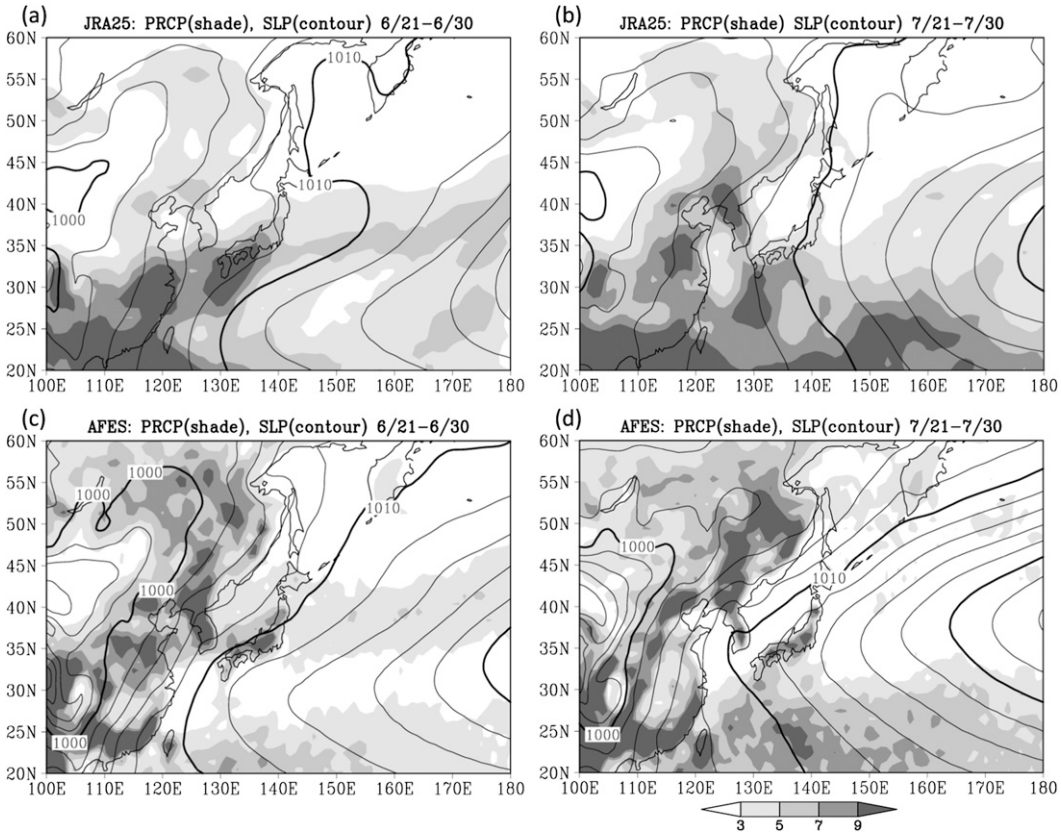

FIG. 4. The 10-day mean of precipitation (shaded, mm day^{-1}) and SLP (contour interval is 2 hPa with 1000, 1010, and 1020 hPa contours thickened) between (left) 21 and 30 June and between (right) 21 and 30 July for (a),(b) JRA-25 and (c),(d) AFES.

(ERA-40; Uppala et al. 2005) and the *World Ocean Atlas 1998* (*WOA98*; Antonov et al. 1998a,b,c; Boyer et al. 1998a,b,c) without motion, respectively. In this study, the first 20-yr integration of the CFES is used. Although CFES shows weak cooling drift in the first 5 yr with a global-mean surface temperature decrease of 0.5 K, it reaches a steady state after that and the baiu rainband remains steady through the first 20 yr. AFES with the same resolution as CFES is integrated with the weekly National Oceanic and Atmospheric Administration (NOAA) optimum interpolation sea surface temperature analysis (OISST; Reynolds et al. 2002) from 1 September 1981 to 31 December 1999. The AFES data from 1 January 1982 are used in this study (AFES).

As observational reference, the 6-hourly Japanese 25-yr Reanalysis (JRA-25; Onogi et al. 2007) is used from 1 January 1985 to 31 December 2004. The daily climatology data of model integrations and observations are used to investigate evolution of the climatological baiu rainband. To estimate precipitation associated with tropical cyclones, best-track data from the Regional Specialized Meteorological Center (RSMC) Tokyo, Japan Meteorological Agency are used.

3. Overview of baiu seasonal march

Figure 1 compares the climatological baiu rainband in June and July between JRA-25 and AFES. In June, the baiu rainband extends over southern China through the southern coast of Japan to the northwestern Pacific Ocean in JRA-25 (Fig. 1a). Precipitation is strong over southern China, the East China Sea, and southwestern Japan, gradually weakening east of Japan over the northwestern Pacific. AFES mostly reproduces the rainband, while it is located more north with weaker precipitation especially over sea than JRA-25 (Fig. 1e). In the baiu season, tropical cyclones contribute to rainfall in East Asia. Figure 1c shows precipitation without that associated with tropical cyclones. The precipitation associated with tropical cyclones is defined as precipitation inside of a circle where wind speed is 30 kt (1 kt $\approx$ 0.51 m s^{-1}) or greater by RSMC best-track data. Although tropical cyclones affect precipitation over the

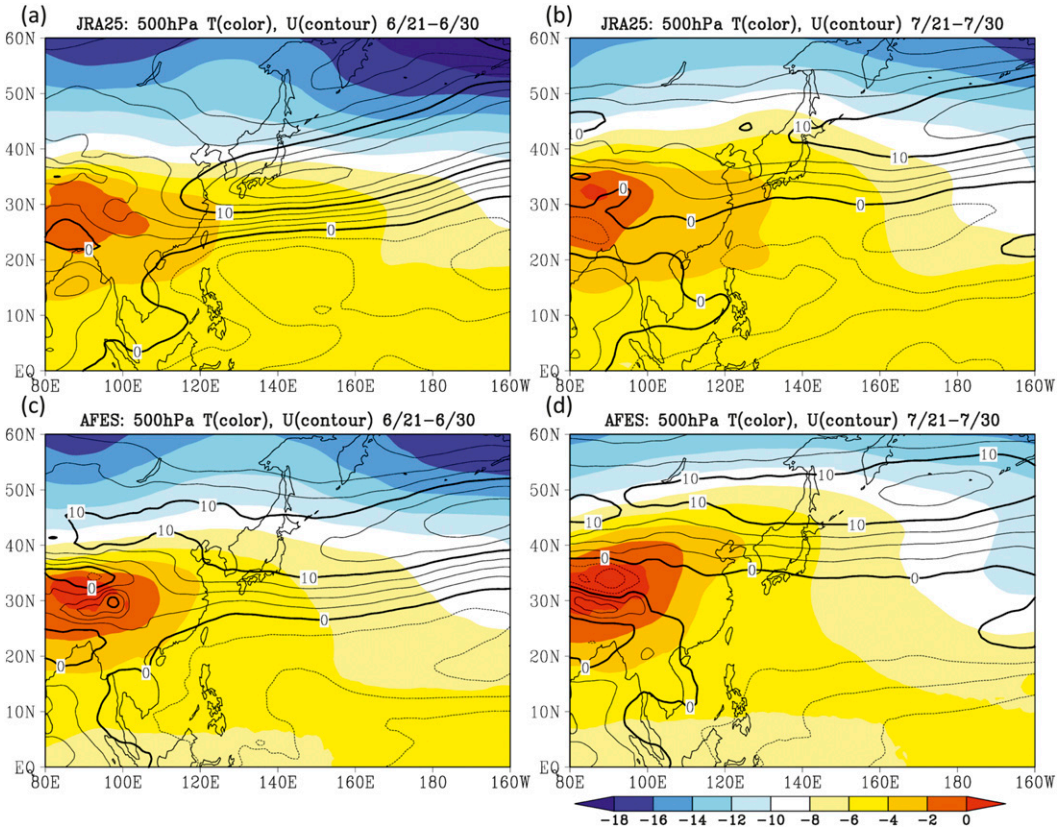

FIG. 5. As in Fig. 4, but for temperature (color, °C) and zonal wind (contour interval is 2.5 m s^{-1} with 0, 10, and 20 m s^{-1} contours thickened) at 500 hPa.

Philippine Sea, the baiu rainband is rarely influenced in June.

In July, AFES differs substantially from observations. In observations the baiu rainband weakens and shifts northward, while precipitation over the subtropics east of the Philippines strengthens (Fig. 1b). The change in subtropics and midlatitude precipitation is connected with the Pacific–Japan pattern (Ueda et al. 1995). In AFES, subtropical convection expands too much northward and occupies the entire warm pool with SST > 28°C, whereas in JRA-25 active convection is kept well south of the northern flank of the warm pool. Perhaps because of the excessive subtropical convection, the continuous midlatitude rainband disappears. Over the Asian continent, rainfall shifts too far northward to cover eastern Siberia (Fig. 1f). The weaker precipitation in the subtropics in AFES may be associated with weak tropical cyclone activity because of the coarser resolution. In JRA-25, tropical cyclones greatly contribute to precipitation over southern China, the East China Seas, and the southern coast of Japan (Fig. 1d). However, the contribution of tropical cyclones is weak to the baiu rainband over east of Japan.

To examine the baiu rainband over the northwestern Pacific east of Japan, precipitation averaged between 140° and 170°E with a 5-day running mean is shown in Fig. 2. Note that the precipitation includes precipitation associated with tropical cyclones because the tropical cyclone's influence is small in the area (Fig. 1). In JRA-25, the baiu rainband is located around 35°N from May to late July and suddenly weakens around late July, while subtropical precipitation becomes active as reported by Ueda et al. (1995) and Sampe and Xie (2010) (Fig. 2a). In AFES, the rainband weakens and shifts northward at the beginning of July three weeks earlier than in JRA-25 (Fig. 2b). The onset of subtropical precipitation (15°–25°N) occurs concurrently with baiu termination.

Sampe and Xie (2010) propose that the horizontal warm temperature advection by the zonal jet in the midtroposphere induces upward motion of the baiu rainband. Here, we test this hypothesis in the seasonal march of vertical motions, horizontal temperature advection, and zonal wind at 500 hPa (Fig. 3). The upward motion band in AFES corresponds well with the horizontal warm advection band, similar to JRA-25 as suggested by Sampe and Xie (2010). The meridional

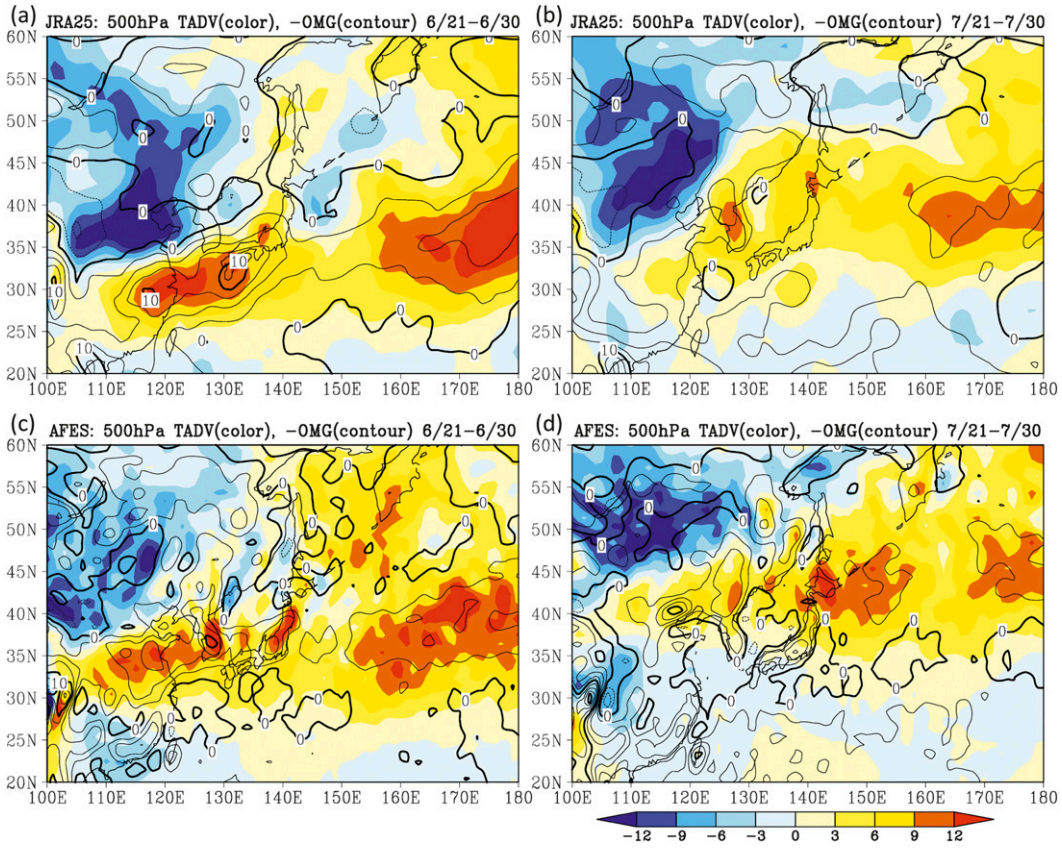

FIG. 6. As in Fig. 4, but for horizontal temperature advection (color, $10^{-6}\,\mathrm{K\,s^{-1}}$) and vertical pressure velocity with negative sign (contour interval is $2.5 \times 10^{-2}\,\mathrm{Pa\,s^{-1}}$ with 0 and $10 \times 10^{-2}\,\mathrm{Pa\,s^{-1}}$ contours thickened) at 500 hPa.

migrations match one another among vertical velocity, warm advection, and the westerly jet. During the northward migration, the upper jet weakens in JRA-25 and AFES. These results suggest that the northward migration of the baiu rainband and resultant termination mostly depend on the westerly jet and horizontal temperature advection, confirming Sampe and Xie's hypothesis in the context of the baiu seasonal variation. However, the magnitude of upward motions and precipitation does not always agree with that of temperature advection.

4. Termination of the baiu rainband

In this section, we focus on the baiu termination to characterize the change before and after. Figure 4 shows 10-day mean fields of sea level pressure (SLP) and precipitation from 21 to 30 June and from 21 to 30 July, periods when the subtropical convection jump takes place in AFES and JRA-25, respectively. In JRA-25, the baiu rainband is located on the north edge of the subtropical high over the Pacific before the baiu termination (Fig. 4a). After the termination the rainband almost disappears and the subtropical ridge shrinks eastward associated with a precipitation increase in the subtropics while in the midlatitudes, the ridge extends over the Sea of Okhotsk (Fig. 4b). In AFES the rainband near Japan is weaker than that in JRA-25 before baiu termination (Fig. 4c). The rainband disappears with a northward shift of the zonal ridge in July (Fig. 4d), associated with a too early onset of the subtropical convection (see Fig. 2b). The results are consistent with the subtropical convective jump of Ueda et al. (1995) and its effect on the baiu rainband.

As a part of the Asian monsoon system, land–sea contrast is important for the baiu rainband formation (Yoshikane et al. 2001). Figure 5 shows temperature and zonal wind at 500 hPa before and after the baiu termination. As suggested by Sampe and Xie (2010), there is a warm region over the Tibetan Plateau and the zonal jet advects the warm temperature through the south of Japan to the northwestern Pacific before the baiu termination in JRA-25 (Fig. 5a). After the baiu termination, the zonal jet shifts northward and weakens (Fig. 5b). In

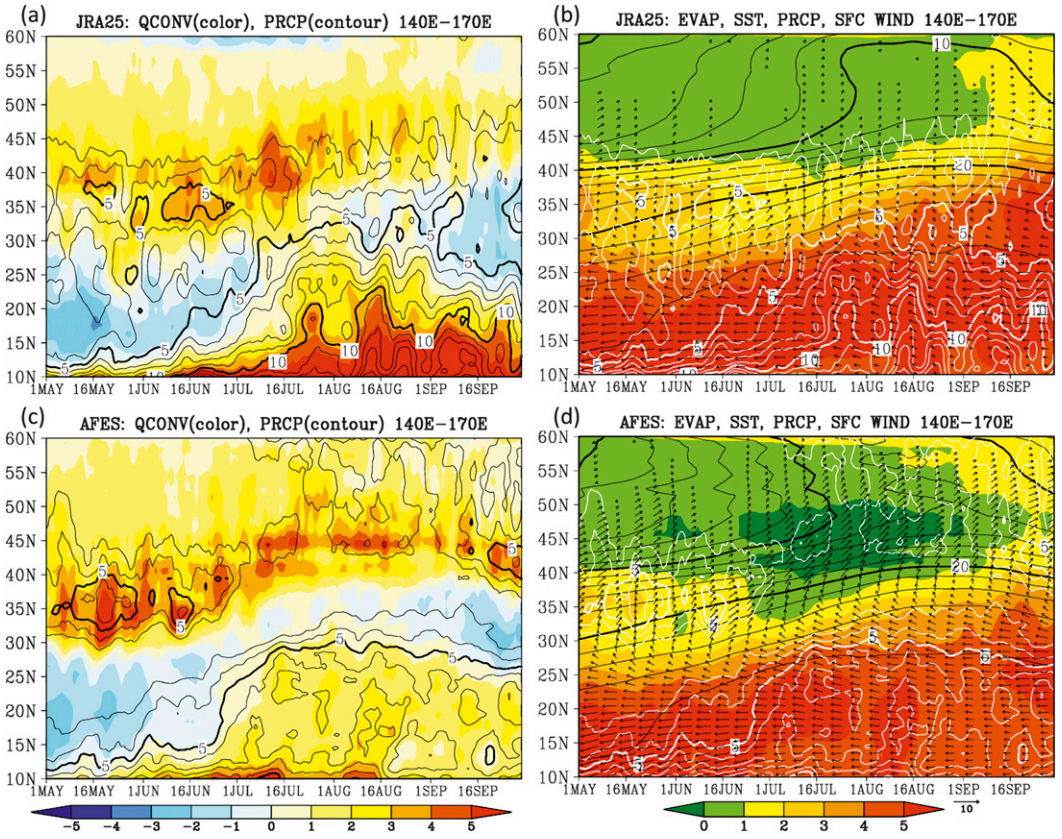

FIG. 7. As in Fig. 2, but for (left) vertical integrated moisture convergence from surface to 250 hPa (color, mm day^{-1}) and precipitation (contours are drawn for the range over 3 mm day^{-1} at every 1 mm day^{-1} with 5 and 10 mm day^{-1} contours thickened) and (right) surface evaporation (color, mm day^{-1}), SST (black contours, contour interval is 2°C with 10° and 20°C contours thickened), surface wind (vectors, m s^{-1}), and precipitation (white contours for the range over 3 mm day^{-1} at every 1 mm day^{-1} with 5 and 10 mm day^{-1} contours thickened) for (a),(b) JRA-25 and (c),(d) AFES.

AFES the temperature fields before and after the baiu termination resemble JRA-25. The westerly jet is too weak before the baiu termination and shifts too much northward after the baiu termination compared to JRA-25 (Figs. 5c,d).

Under these large-scale environments, horizontal temperature advection and upward motion show sharp changes before and after the baiu termination in JRA-25 and AFES (Fig. 6). Before the baiu termination they peak in a zonal band from southern China to the southern coast of Japan and the northwestern Pacific anchoring the baiu rainband in JRA-25 as suggested by Sampe and Xie (2010) (Figs. 6a, 4a). After the baiu termination they weaken over southern China and the southern coast of Japan, and horizontal warm advection is large over northern Japan and the northwestern Pacific (Fig. 6b). The AFES shows similar distributions and seasonal evolution to JRA-25 with the band of maximum displaced northward as a result of the biases of the westerly jet (Figs. 6c,d). These results suggest that the general location and seasonal evolution of the baiu rainband is consistent with the hypothesis by Sampe and Xie (2010). However, there are inconsistencies between warm advection, upward motion, and precipitation in JRA-25 and AFES. In late June the rainband and upward motion in JRA-25 over the northwestern Pacific are weaker than that over southern China and the southern coast of Japan (Fig. 4a) in spite of a similar magnitude in warm advection (Fig. 6a). In AFES, also, the warm advection remains strong and is organized into a zonal band over northern Japan and the northwestern Pacific while rain and upward motion are disorganized and scattered at the end of July (Figs. 4d, 6d). These inconsistencies indicate other factors that contribute to the precipitation amount and upward motion amplitude of the baiu rainband. The SST frontal effect on convection has been documented along the Gulf Stream (Minobe et al. 2008, 2010; Kuwano-Yoshida et al. 2010b; Chelton and

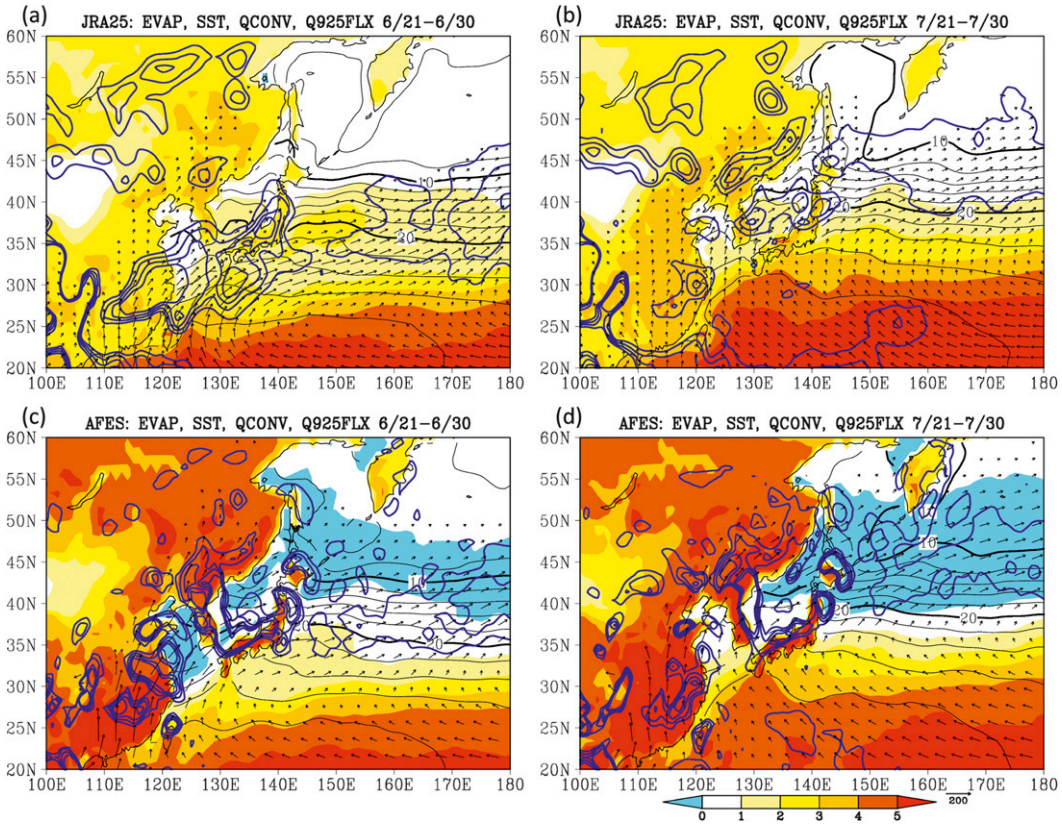

FIG. 8. As in Fig. 4, but for surface evaporation (color, mm day^{-1}), SST (black contours, contour interval is 2°C with 10° and 20°C contours thickened), moisture flux at 925 hPa (vectors over 20 kg kg^{-1} m s^{-1}), and vertically integrated moisture convergence (3, 5, 7, and 9 mm day^{-1} are plotted with blue contours).

Xie 2010) and Kuroshio (Xu et al. 2011; Sasaki et al. 2012).

5. Moisture budget of the baiu rainband

The previous section suggested that the baiu rainband strength cannot be fully explained by horizontal temperature advection in the midtroposphere alone, although the meridional shift of the baiu rainband is associated with the upper jet shift. Moisture budget analysis is useful to understand the precipitation amount. The moisture budget equation can be written as follows:

$$\int_{250\text{hPa}}^{\text{SLP}} \frac{\partial q}{\partial t}\, dp = \int_{250\text{hPa}}^{\text{SLP}} -\nabla \cdot (q\mathbf{V})\, dp + E - P, \quad (1)$$

where q is specific humidity, t is time, p is pressure, $\mathbf{V}$ is the horizontal velocity vector, E is surface evaporation, and P is precipitation. Because the left-hand side in Eq. (1) is negligible for the long-term mean, the terms in the right-hand side are analyzed here.

Figure 7 shows the seasonal march of the moisture budget over the northwestern Pacific. The baiu rainband mostly overlaps with the maximum of vertical integrated moisture convergence for JRA-25 and AFES. As the baiu rainband weakens and shifts northward in JRA-25 and AFES, precipitation weakens considerably more than moisture convergence (Figs. 7a,c). The moisture convergence zone shifts northward to the north of the large meridional SST gradient zone (called the SST front, hereafter), where surface evaporation vanishes in JRA-25 and AFES (Figs. 7b,d). Surface evaporation shows a sharp decrease across the SST front because the prevailing southwesterlies advect warm and humid air over the cold ocean surface, causing fog north of the SST front (Tokinaga et al. 2009). These results suggest that the SST modulation of the surface evaporation contributes to the strength of the baiu rainband, while horizontal convergence associated with warm advection–induced upward motion sets the location of the baiu rainband.

In JRA-25 during the baiu season, the band of moisture convergence forms over southern China, the East

China Sea, southern Japan, and east of Japan with the southwesterly moisture flux (Fig. 8a). Beneath the convergence zone, surface evaporation is large. After the baiu rainband termination, the moisture convergence zone shifts north of 40°N where the SST front is located (Fig. 8b). Surface evaporation under the moisture convergence zone is nearly zero because of cold SST and moist air advection from south. As a result, precipitation weakens. Precipitation is weak over the East China Sea in AFES during the baiu season (Fig. 4c). While the upper warm advection is displaced north over the Yellow Sea (Fig. 6c) and large moisture flux flows in from the tropics, the surface evaporation is negative over the Yellow and the East China Seas. In late July, the moisture convergence zone shifts north of 40°N where the surface evaporation is negative in AFES (Fig. 8d), resulting in weak precipitation (Fig. 4c). The results support that upper-level warm advection controls precipitation location, while the precipitation amount depends on surface evaporation.

The moisture budget analysis shows that the relative location of the baiu rainband to the SST front affects the baiu rainband strength before and after the baiu termination. Since the timing of baiu termination shows large interannual variations (Kosaka et al. 2011), a simple climatological average may not capture the baiu termination characteristics. We use the maximum of horizontal temperature advection at 500 hPa in a 5-day running mean and zonal mean between 140° and 170°E (TADV500) as an index of the dynamical baiu location for each year. The maximum is searched between 20° and 60°N. Figure 9 shows the daily frequency of the TADV500 maximum as a function of time and latitude. A frequency of 1 means that the TADV500 has its maximum at a particular latitude at a particular day in 1 day among 20 yr. Note that the frequency is also operated by a 5-day running mean. In JRA-25 the frequency peak is consistent with the climatological maximum of TADV500 in Fig. 3c. A second peak appears from late June to the first half of July along 42°N (Fig. 9a), associated with years with earlier baiu termination than the climatology. In AFES, the double peaks are clear in June followed by the single peak in July (Fig. 9b).

To analyze the relation between the dynamical baiu location and the SST front, two composites relative to the latitude of TADV500 maximum are made: one is for the TADV500 maximum being located between 40° and 50°N (denoted as N) and the other between 30° and 40°N (denoted as S). The composites S and N correspond to the composites for the periods during and after the baiu, respectively. Figure 10 shows N and S composites of the moisture budget equation averaged between 140° and 170°E. The origin of the horizontal axis (0°) indicates the

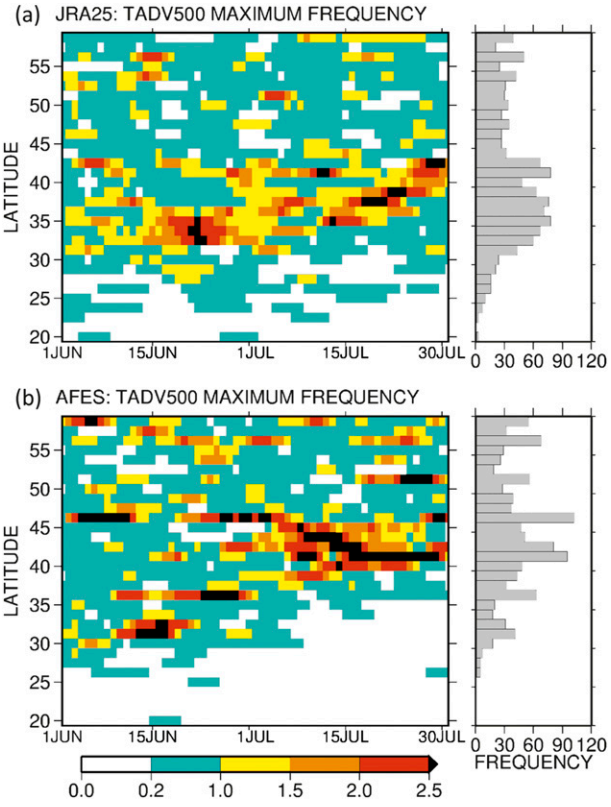

FIG. 9. (left) Daily appearance frequency of TADV500 maximum (detailed definition is described in text) between 1 June and 31 July (color, 20 yr^{-1}) and (right) its cumulated frequency in June and July for (a) JRA-25 and (b) AFES.

TADV500 maximum. In the N composite, the precipitation peak under the TADV500 maximum is smaller than the moisture convergence peak (Fig. 10a). The residuum of moisture is explained by the moisture tendency term, the left-hand side of Eq. (1), associated with the seasonal transition (not shown). Evaporation is almost zero because of the SST front. In contrast, the precipitation peak is clear and as large as the moisture convergence under the TADV500 maximum in the S composite (Fig. 10b). Evaporation is large to the south of the TADV500 maximum where the moisture diverges. In the difference between the S and N composites, the SST is higher under the TADV500 maximum in the S composite (Fig. 10c). The moisture convergence accounts for ⅔ of the precipitation difference and evaporation for ⅓. In addition, evaporation south of the TADV500 maximum compensates the moisture divergence. Since southwesterly wind prevails there, the evaporated moisture is transported under the TADV500 maximum, maintaining the baiu rainband. Similar features can be seen in AFES. In the N composite, the moisture convergence shows a peak under the TADV500

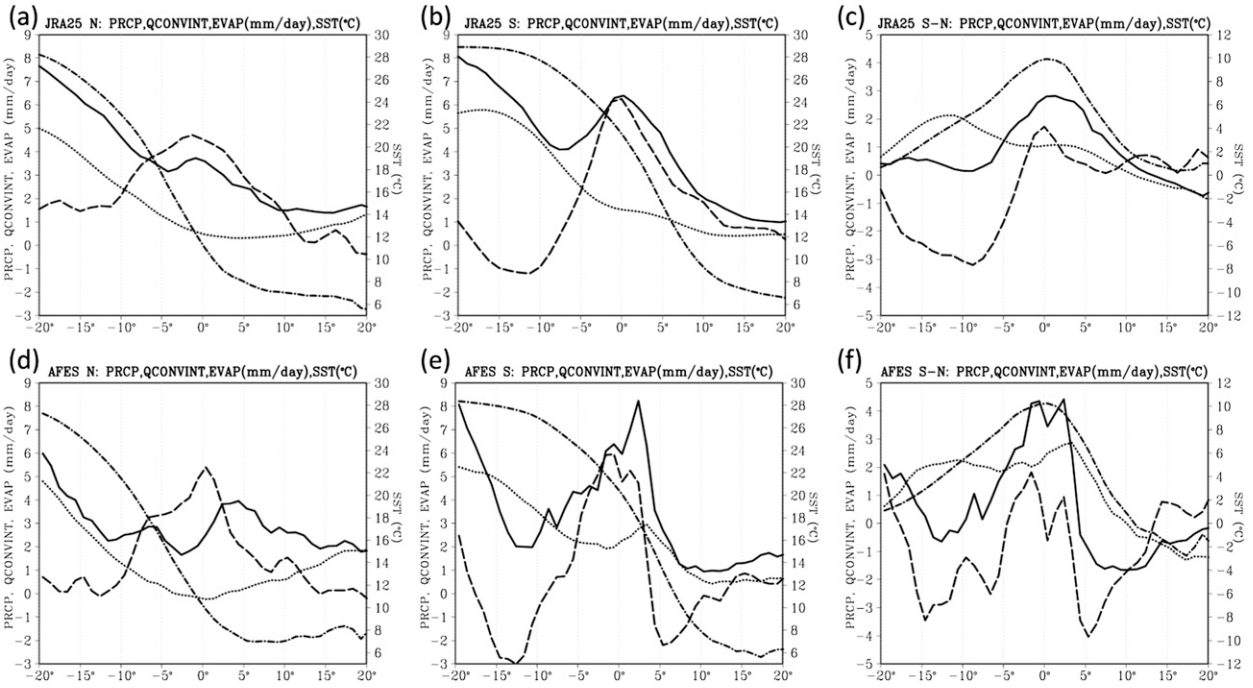

FIG. 10. Moisture budget analysis averaged between 140° and 170°E for (top) JRA-25 and (bottom) AFES. Composites when TADV500 maximum is located (a),(d) between 40° and 50°N (N), (b),(e) between 30° and 40°N (S), and (c),(f) difference between S and N. Precipitation (mm day^{-1}, solid line), vertical integrated horizontal moisture convergence (mm day^{-1}, dashed line), surface evaporation (mm day^{-1}, dotted line), and SST (°C, dotted–dashed line, right axis).

maximum and the evaporation is almost zero there, while precipitation peak slightly shifts northward (Fig. 10d). In the S composite, the moisture convergence and evaporation maintain the large precipitation peak under the TADV500 maximum (Fig. 10e). The difference between S and N composites shows that the moisture convergence and evaporation each contribute to a half of the precipitation difference because evaporation under the TADV500 maximum is larger than JRA-25 (Fig. 10f). These results suggest that the baiu rainband is not only maintained by the dynamical forcing of horizontal temperature advection at the midtroposphere, but that the sea surface evaporation is also significant to maintain the baiu rainband. The baiu rainband termination occurs when the TADV500 maximum shifts north of the SST front, where SST and the moisture supply from the sea surface are both weak.

6. Baiu rainband in CFES

The previous section shows that the relative position of the TADV500 maximum to the SST front is important to the baiu rainband maintenance and the baiu termination. In this section, we focus on the baiu rainband in CFES to understand what controls the baiu rainband in GCMs. Figure 11 shows the baiu's seasonal march over the northwestern Pacific in CFES. The baiu rainband continues from May to September over the SST front without the baiu termination in contrast to JRA-25 and AFES (Fig. 11a). While the TADV500 maximum gradually moves northward, as in JRA-25 and AFES, it never goes beyond 40°N (Fig. 11b). The moisture budget analysis shows that the rainband locates over the SST front and the moisture flux converges under the TADV500 maximum from the south (Figs. 11c,d). These results suggest that the baiu rainband in CFES continues without a clear termination because the TADV500 maximum stays over the warm side of the SST front, supported by a large moisture supply from the sea surface.

The stagnation of the TADV500 maximum in CFES may be caused by several mechanisms. One mechanism is the SST bias in CFES. The cold SST bias in the subtropics suppresses the subtropical convection jump, allowing only a weak northward migration of the midlatitude jet (Fig. 11a). Okajima and Xie (2007) noted a similar evolution of SST anomalies and interaction with summer convection over the northwestern Pacific in response to orographic forcing by the Tibetan Plateau. Second, the cold SST bias is larger in higher latitudes, making a sharper SST front in midlatitudes. The

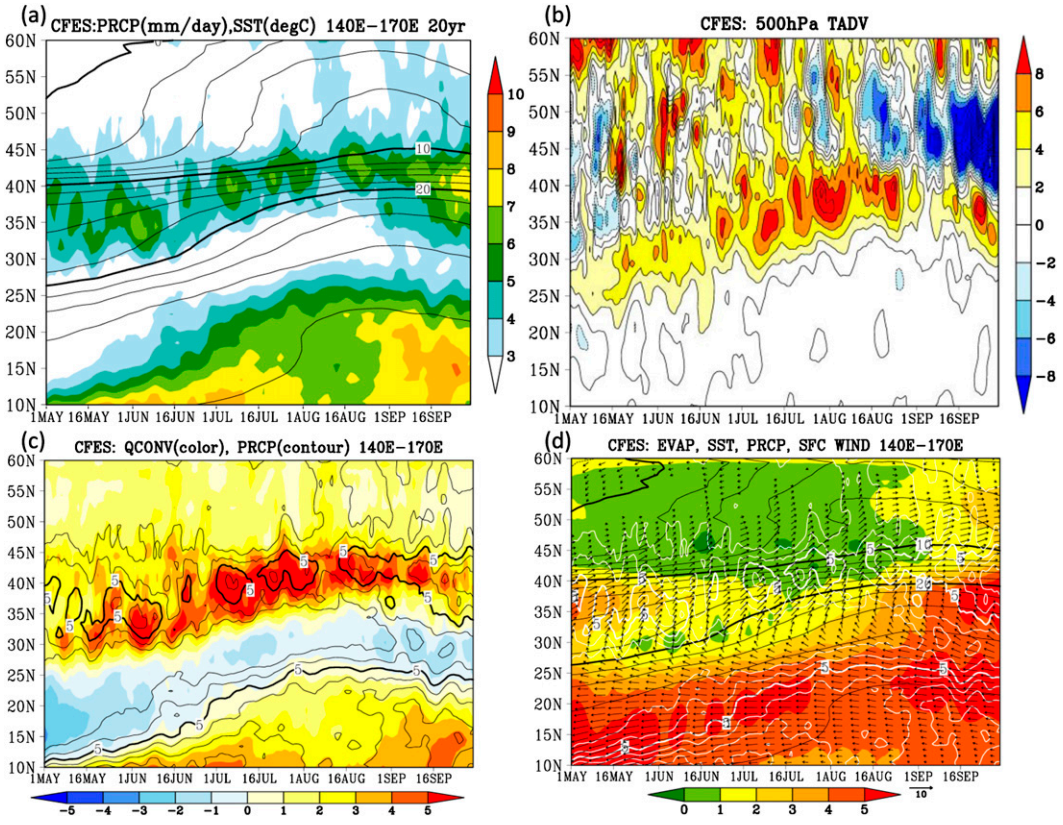

FIG. 11. Seasonal evolution of the baiu rainband in CFES. (a) Precipitation (color, mm day^{-1}) and SST (contour interval is 2°C with 10° and 20°C contours thickened) averaged between 140° and 170°E with 5-day running mean from 1 May to 30 September; (b) TADV500 (10^{-6} K s^{-1}); (c) vertical integrated moisture convergence from surface to 250 hPa (color, mm day^{-1}) and precipitation (contours are drawn for the range over 3 mm day^{-1} at every 1 mm day^{-1} with 5 and 10 mm day^{-1} contours thickened); and (d) surface evaporation (color, mm day^{-1}), SST (black contour, contour interval is 2°C with 10° and 20°C contours thickened), surface wind (vectors, m s^{-1}), and precipitation (white contours for the range over 3 mm day^{-1} at every 1 mm day^{-1} with 5 and 10 mm day^{-1} contours thickened).

strong SST front anchors and strengthens the midlatitude atmospheric jet. As a result, the warm advection by the midlatitude jet cannot move northward across the SST front. These results suggest the importance of the westerly jet and SST for the baiu rainband and subtropical convection in AOGCMs.

7. Summary and conclusions

We have compared the baiu rainbands in JRA-25 and a pair of AGCM and AOGCM that share the same atmospheric component. Compared to JRA-25, the baiu rainband terminates about 1 month early in AFES while it persists through the summer in CFES. The difference in the baiu rainbands between AFES and CFES is closely tied to subtropical convection to the south, consistent with Ueda et al. (1995, 2009). Our analysis shows that the midtropospheric horizontal thermal advection mechanism of Sampe and Xie (2010) partly explains the baiu termination in AFES and the lack of it in CFES. This mechanism alone is insufficient and the rapid northward decrease in ocean evaporation across the midlatitude SST front is necessary to account for the abrupt precipitation decrease along the westerly jet after the baiu termination. CFES suffers large cold SST biases, which affect ocean evaporation and the position and intensity of the westerly jet and thereby the baiu rainband location and strength.

Based on the findings, we propose a conceptual model of the baiu rainband termination as summarized in Fig. 12. During the baiu season, the rainband is maintained by upward motion induced by midtroposphere warm advection and surface evaporation south of the SST front (Fig. 12a). At the baiu termination, the midtroposphere jet shifts northward over the cold SST north of the SST front where surface evaporation is suppressed. Changes in moisture convergence are small before and after the baiu termination. As a result, the rainband weakens because of the decreased moisture supply despite upward motion induced by the band of midtropospheric warm temperature advection (Fig. 12b). The northward shift

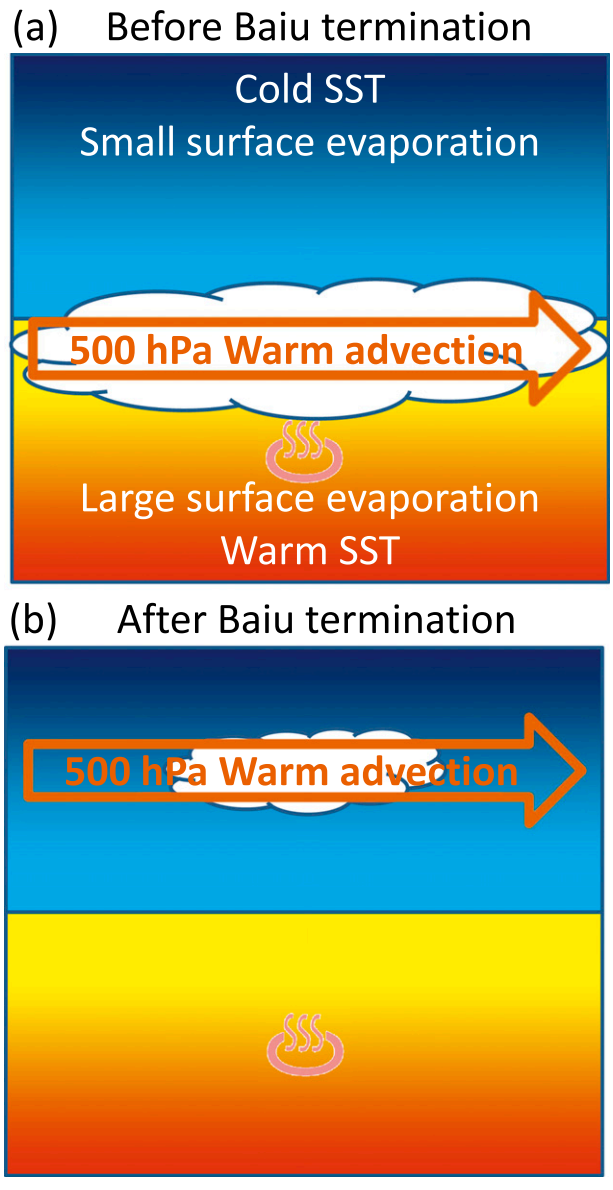

FIG. 12. A revised conceptual model of baiu (a) before baiu termination and (b) after baiu termination.

of the westerly jet may be triggered by the onset of subtropical convection as in Ueda and Yasunari (1996). Our results illustrate that surface conditions and the midtropospheric jet are important for the baiu rainband.

Climate models perform poorly and show large disagreement between them in baiu simulation (Ninomiya 2011). While the baiu's relationship to the upper jet has recently been discussed, few studies have examined surface evaporation near baiu and its effect on the rainband. Our analysis and the conceptual model provide a useful framework to assess climate models and understand future changes in the baiu models project.

Acknowledgments. AFES and CFES integrations were performed on the Earth Simulator with support of JAMSTEC. This work is supported by the Japanese Ministry of Education, Culture, Sports, Science and Technology (MEXT) through a Grant-in-Aid for Scientific Research in Innovative Areas 2205 "Hot Spots in Climate System," the U.S. NSF, and NASA.

REFERENCES

Akiyama, T., 1973: The large-scale aspects of the characteristic features of the baiu front. *Pap. Meteor. Geophys.,* **24,** 157–188.

Antonov, J. I., S. Levitus, T. P. Boyer, M. E. Conkright, T. O'Brien, and C. Stephens, 1998a: *Temperature of the Atlantic Ocean.* Vol. 1, *World Ocean Atlas 1998,* NOAA Atlas NESDIS 27, 166 pp.

——, ——, ——, ——, ——, and ——, 1998b: *Temperature of the Pacific Ocean.* Vol. 2, *World Ocean Atlas 1998,* NOAA Atlas NESDIS 28, 166 pp.

——, ——, ——, ——, ——, ——, and B. Trotsenko, 1998c: *Temperature of the Indian Ocean.* Vol. 3, *World Ocean Atlas 1998,* NOAA Atlas NESDIS 29, 166 pp.

Boyer, T. P., S. Levitus, J. I. Antonov, M. E. Conkright, T. O'Brien, and C. Stephens, 1998a: *Salinity of the Atlantic Ocean.* Vol. 4, *World Ocean Atlas 1998,* NOAA Atlas NESDIS 30, 166 pp.

——, ——, ——, ——, ——, and ——, 1998b: *Salinity of the Pacific Ocean.* Vol. 5, *World Ocean Atlas 1998,* NOAA Atlas NESDIS 31, 166 pp.

——, ——, ——, ——, ——, ——, and B. Trotsenko, 1998c: *Salinity of the Indian Ocean.* Vol. 6, *World Ocean Atlas 1998,* NOAA Atlas NESDIS 32, 166 pp.

Chelton, D. B., and S.-P. Xie, 2010: Coupled ocean-atmosphere interaction at oceanic mesoscales. *Oceanography,* **23** (4), 52–69.

Enomoto, T., A. Kuwano-Yoshida, N. Komori, and W. Ohfuchi, 2008: Description of AFES 2: Improvements for high-resolution and coupled simulations. *High Resolution Numerical Modelling of the Atmosphere and Ocean,* K. Hamilton and W. Ohfuchi, Eds., Springer, 77–97.

Kawatani, Y., and M. Takahashi, 2003: Simulation of the baiu front in a high resolution AGCM. *J. Meteor. Soc. Japan,* **81,** 113–126.

Kodama, Y., 1992: Large-scale common features of subtropical precipitation zones (the baiu frontal zone, the SPCZ, and the SACZ). Part I: Characteristics of subtropical frontal zones. *J. Meteor. Soc. Japan,* **70,** 813–836.

Komori, N., K. Takahashi, K. Komine, T. Motoi, X. Zhang, and G. Sagawa, 2005: Description of sea-ice component of Coupled Ocean–Sea-Ice Model for the Earth Simulator (OIFES). *J. Earth Simul.,* **4,** 31–45.

——, A. Kuwano-Yoshida, T. Enomoto, H. Sasaki, and W. Ohfuchi, 2008: High-resolution simulation of global coupled atmosphere–ocean system: Description and preliminary outcomes of CFES (CGCM for the Earth Simulator). *High Resolution Numerical Modelling of the Atmosphere and Ocean,* K. Hamilton and W. Ohfuchi, Eds., Springer, 241–260.

Kosaka, Y., S.-P. Xie, and H. Nakamura, 2011: Dynamics of interannual variability in summer precipitation over East Asia. *J. Climate,* **24,** 5435–5453.

Kuwano-Yoshida, A., T. Enomoto, and W. Ohfuchi, 2010a: An improved PDF cloud scheme for climate simulations. *Quart. J. Roy. Meteor. Soc.,* **136,** 1583–1597.

——, S. Minobe, and S.-P. Xie, 2010b: Precipitation response to the Gulf Stream in an atmospheric GCM. *J. Climate,* **23,** 3676–3698.

Matsumoto, S., K. Ninomiya, and S. Yoshizumi, 1971: Characteristic features of ''baiu'' front associated with heavy rainfall. *J. Meteor. Soc. Japan,* **49,** 267–281.

Meehl, G. A., C. Covey, K. E. Taylor, T. Delworth, R. J. Stouffer, M. Latif, B. McAvaney, and J. F. B. Mitchell, 2007: The WCRP CMIP3 multimodel dataset: A new era in climate change research. *Bull. Amer. Meteor. Soc.,* **88,** 1383–1394.

Minobe, S., A. Kuwano-Yoshida, N. Komori, S.-P. Xie, and R. J. Small, 2008: Influence of the Gulf Stream on the troposphere. *Nature,* **452,** 206–209.

——, M. Miyashita, A. Kuwano-Yoshida, H. Tokinaga, and S.-P. Xie, 2010: Atmospheric response to the Gulf Stream: Seasonal variations. *J. Climate,* **23,** 3699–3719.

Ninomiya, K., 1984: Characteristics of baiu front as a predominant subtropical front in the summer Northern Hemisphere. *J. Meteor. Soc. Japan,* **62,** 880–894.

——, 2009: Characteristics of precipitation in the meiyu-baiu season in the CMIP3 20th century climate simulations. *J. Meteor. Soc. Japan,* **87,** 829–843.

——, 2011: Characteristics of the meiyu and baiu frontal precipitation zone in the CMIP3 20th century simulation and 21st century projection. *J. Meteor. Soc. Japan,* **89,** 151–159.

——, and T. Akiyama, 1992: Multi-scale features of baiu, the summer monsoon over Japan and the East Asia. *J. Meteor. Soc. Japan,* **70,** 467–495.

——, T. Nishimura, W. Ohfuchi, T. Suzuki, and S. Matsumura, 2002: Features of the baiu front simulated in an AGCM (T42L52). *J. Meteor. Soc. Japan,* **80,** 697–716.

Numaguti, A., M. Takahashi, T. Nakajima, and A. Sumi, 1997: Description of CCSR/NIES atmospheric general circulation model. *Study on the Climate System and Mass Transport by a Climate Model, Center for Global Environmental Research Supercomputer Monogr.,* Vol. 3, National Institute for Environmental Studies, 1–48.

Ohfuchi, W., and Coauthors, 2004: 10-km mesh mesoscale resolving simulations of the global atmosphere on the Earth Simulator—Preliminary outcomes of AFES (AGCM for the Earth Simulator. *J. Earth Simul.,* **1,** 8–34.

——, H. Sasaki, Y. Masumoto, and H. Nakamura, 2007: ''Virtual'' atmospheric and oceanic circulation in the Earth Simulator. *Bull. Amer. Meteor. Soc.,* **88,** 861–866.

Okajima, H., and S.-P. Xie, 2007: Orographic effects on the northwestern Pacific monsoon: Role of air-sea interaction. *Geophys. Res. Lett.,* **34,** L21708, doi:10.1029/2007GL032206.

Onogi, K., and Coauthors, 2007: The JRA-25 Reanalysis. *J. Meteor. Soc. Japan,* **85,** 369–432.

Pacanowski, R. C., and S. M. Griffies, 2000: MOM 3.0 manual. National Oceanic and Atmospheric Administration/Geophysical Fluid Dynamics Laboratory, 680 pp.

Reynolds, R. W., N. A. Rayner, T. M. Smith, D. C. Stokes, and W. Wang, 2002: An improved in situ and satellite SST analysis for climate. *J. Climate,* **15,** 1609–1625.

Saito, N., 1985: Quasi-stationary waves in mid-latitudes and the baiu in Japan. *J. Meteor. Soc. Japan,* **63,** 983–995.

Sampe, T., and S.-P. Xie, 2010: Large-scale dynamics of the meiyu-baiu rainband: Environmental forcing by the westerly jet. *J. Climate,* **23,** 113–134.

Sasaki, Y. N., S. Minobe, T. Asai, and M. Inatsu, 2012: Influence of the Kuroshio in the East China Sea on the early summer (baiu) rain. *J. Climate,* **25,** 6627–6645.

Taguchi, B., H. Nakamura, M. Nonaka, N. Komori, A. Kuwano-Yoshida, K. Takaya, and A. Goto, 2012: Seasonal evolutions of atmospheric response to decadal SST anomalies in the North Pacific subarctic frontal zone: Observations and a coupled model simulation. *J. Climate,* **25,** 111–139.

Tochimoto, E., and T. Kawano, 2012: Development processes of baiu frontal depressions. *SOLA,* **8,** 9–12.

Tokinaga, H., Y. Tanimoto, S.-P. Xie, T. Sampe, H. Tomita, and H. Ichikawa, 2009: Ocean frontal effects on the vertical development of clouds over the western North Pacific: In situ and satellite observations. *J. Climate,* **22,** 4241–4260.

Ueda, H., and T. Yasunari, 1996: Maturing process of the summer monsoon over the western North Pacific: A coupled ocean/atmosphere system. *J. Meteor. Soc. Japan,* **74,** 493–508.

——, ——, and R. Kawamura, 1995: Abrupt seasonal change of large-scale convective activity over the western Pacific in the northern summer. *J. Meteor. Soc. Japan,* **73,** 795–809.

——, M. Ohba, and S.-P. Xie, 2009: Important factors for the development of the Asian–northwest Pacific summer monsoon. *J. Climate,* **22,** 649–669.

Uppala, S. M., and Coauthors, 2005: The ERA-40 Re-Analysis. *Quart. J. Roy. Meteor. Soc.,* **131,** 2961–3012.

Xu, H., M. Xu, S.-P. Xie, and Y. Wang, 2011: Deep atmospheric response to the spring Kuroshio over the East China Sea. *J. Climate,* **24,** 4959–4972.

Yoshikane, T., F. Kimura, and S. Emori, 2001: Numerical study on the baiu front genesis by heating contrast between land and ocean. *J. Meteor. Soc. Japan,* **79,** 671–686.